A comprehensive algorithm using a fixed toroidal magnetic field for plasma equilibrium with flow

A. Djellouli

Theoretical Physics Laboratory, Faculty of Sciences,
Abou Bekr Belkaid University, 13000, Tlemcen, Algeria.
e-mail: djellouli.amina@univ-tlemcen.dz

A. Rachida Senoudi

Department of physics, Faculty of Sciences,
Abou Bekr Belkaid University, 13000, Tlemcen, Algeria.
e-mail: assiarachida.senoudi@univ-tlemcen.dz

Received 8 May 2025; accepted 1 July 2025

This study presents a finite element method (FEM) solver developed to compute the steady equilibrium of an axisymmetric plasma with toroidal flow. The main objective of the algorithm is to determine the free parameters of the toroidal current source using two key constraints: the measured toroidal magnetic field (TMF) at the magnetic axis and the global error defined by Hilbert. To ensure the accuracy of the performed code, the validation was performed using typical parameters of the JT-60SA (Japan Torus-60 Super Advanced) experiments, and its TMF equal to $B_0 = 2.25$ T. The algorithm reveals a reconstruction error of approximately 0.1% for the flux function. The results also indicate that for a Mach number at the major radius between 0.2 and 0.3, the maximum plasma current reaches 5.5 MA. Furthermore, the normalized beta and safety factor are around 3, the average poloidal beta is 0.8, the normalized inductance is 0.75, and the toroidal frequency (ω) at the major radius is 63 krad/s. These results are found in good agreement with experimental data. Additionally, the study provides a quantitative assessment of how the toroidal flow affects plasma parameters and demonstrates the relationship between poloidal beta and rotation velocity.

Keywords: MHD equilibrium; toroidal mach number; fixed toroidal magnetic field; finite element method.

DOI: https://doi.org/10.31349/RevMexFis.71.061501

1. Introduction

Tokamaks are the primary devices for achieving controlled thermonuclear fusion using magnetic confinement. The first step in the modeling and analysis involves magnetohydrodynamic (MHD) equilibrium calculations, typically based on the Grad-Shafranov equation (GS) [1,2], which assumes a static, and axisymmetric plasma. However, this assumption does not accurately reflect experimental observations, where significant toroidal and poloidal rotations often occur even without external momentum sources. Advances in plasma injection technics in the early 1980s allowed toroidal rotation velocities in tokamaks to reach 100-150 km/s [3]. These flows are not merely secondary phenomena; they can greatly influence plasma stability [4,5] and affect critical confinement structures such as the magnetic separatrix and X-points, which are vital for effective plasma containment.

Earlier studies primarily incorporated plasma rotation in stability analyses, while often neglecting its role in equilibrium modeling. However, several key studies [6-13] have emphasized the necessity of including rotation in both stability and equilibrium equations to achieve a more consistent and realistic representation of plasma behavior in tokamaks. Due to its complexity, fully integrating flow effects into equilibrium formulations remains a significant challenge in current research. To address this, the GS equation has been generalized by adding inertial terms associated with plasma flow, resulting in the so-called generalized Grad-Shafranov (GGS) equation.

The GGS equation requires the definition of two arbitrary scalar functions: plasma kinetic pressure (P) and the diamagnetic function (F), which are two components of the toroidal current density and cannot be self-consistently determined within the MHD model.

Instead, "free" functions are either determined from experimental measurements to adjust the parameters of the MHD equilibrium model, using various existing simulation codes such as CHEASE [14], FLOW [15], M3D, and ECOM [16]. Experimental measurements used for equilibrium studies typically include plasma shape, plasma current, magnetic field data, and pressure profiles derived from temperature and density diagnostics. Alternatively, simple analytical profiles can be used to approximate realistic plasma conditions. However, arbitrarily specifying current source terms to analyze toroidal velocity effects does not provide reliable control over plasma parameters. A direct approach to control the current profile involves establishing specific physical plasma parameters as fixed constraints. These may include the total plasma current, poloidal plasma beta, safety factor, or maximum plasma pressure. The current source is then modified to align with these predetermined experimental parameters. This approach has been explored in several publications [17-19].

Theoretical studies [6] have demonstrated that key plasma quantities, including the total plasma current, depend on the toroidal Mach number (the ratio of plasma velocity to sound speed). This suggests that, instead of traditional constraints such as plasma current, safety factors, or pressure at the magnetic axis, it may be possible to consider an alternative constraint that, to our knowledge, has not been previously explored: the on-axis toroidal magnetic field (TMF). Using the toroidal magnetic field (TMF) as a constraint provides a clear and consistent method for selecting current profiles in numerical studies of steady-state plasma equilibrium.

This is particularly relevant, as the toroidal magnetic field is often considered constant over time or within a given operating regime, especially in static equilibrium calculations, where dynamic variations are neglected. For example, the JT-60SA features eighteen D-coils designed to operate at 25.7 kA, producing a field of 2.25 T on the toroidal axis surrounding the tokamak [22]. Since the problem involves the determination of two free parameters, it is necessary to introduce a second constraint to fully define the equilibrium. To address this, an exact analytical solution is used as a reference. This approach not only provides a consistent framework for selecting the additional constraint but also ensures that the numerical equilibrium remains physically meaningful and closely aligned with known theoretical results.

This work presents a computational framework for numerically calculating current density while satisfying two specific constraints. The first constraint keeps the TMF at the magnetic axis at a constant value that corresponds to measured data. The second constraint reduces the overall error in Hilbert space, bringing the exact and numerical solutions of the GGS equation into alignment. Following this process, various output parameters can be determined. Plasma equilibrium is treated either by imposing a fixed boundary [19,23] or by adopting a free boundary approach [24]. While using a fixed boundary is common practice in this field, it limits the modeling of certain dynamic effects. However, this choice is suitable for the study's objective, which focuses on understanding the impact of flow on internal plasma parameters. The computational domain uses the smooth D-shaped Miller parameterization [25,26], which provides a compact expression for the flux surface contour. This parameterization is also capable to generate circular cross-section configurations However, it relies on an asymptotic expansion that assumes a small inverse aspect ratio, $\epsilon = a/R_0$, where R_0 and a denote the major and minor radius of the torus, respectively. We have used typical plasma parameters for the JT-60SA (Japan Torus-60 Super Advanced), listed in Table I [20], to validate our code.

The article is organized as follows: Section 2 explains the procedure for introducing toroidal flow into the GS equation, based on the assumptions of Maschke and Perrin [6] and Ivanov [8]. Section 3 describes the computational domain. Section 4 provides the exact analytical solution, along with the boundary conditions. Section 5 outlines the numerical method encompass with the Finite Element Method (FEM) and an overview of the proposed computational framework. Section 6 validates the algorithm, comparing the exact solution with the numerical equilibrium in a full-current inductive plasma scenario for the JT-60SA. Finally, Sec. 7 presents a quantitative analysis of the effect of toroidal flow on key internal parameters of the equilibrium plasma. In the last section, our conclusions and perspectives are presented.

TABLE I. Typical parameters of Tokamaks JT-60SA [20] and ITER [21].

parameters	JT-60SA full I_{P}	ITER like -shape inductive
Plasma current I_{P} (MA)	5.50	4.60
Toroidal magnetic field B_0 (T)	2.25	2.28
Safety factor q_{95}	3.00	3.20
Major radius R_0 (m)	2.96	2.93
Minor radius a (m)	1.18	1.14
Aspect ratio A	2.5	2.6
Elongation κ_x/κ_{95}	1.87/1.72	1.81/1.70
Triangularity δ_x/δ_{95}	0.50/0.40	0.41/0.33
Shape factor (S=$q_{95}I_{\mathrm{P}}/(aB_0)$)	6.30	5.70
Normalized Beta β_{N}(mT/MA)	3.1	2.8
Electron density $\langle n_{\mathrm{e}}\rangle,\ n_{\mathrm{e}}(0)$ ($10^{20}\mathrm{m}^{-3}$)	0.56/0.77	0.81/1.11
Temperature $\langle T_{\mathrm{e}}\rangle, T_{\mathrm{e}}(0)$ (keV)	6.3/13.5	3.7/8
Plasma volume (m^3)	131	122

2. Formulation of the general equilibrium

The magnetohydrodynamic (MHD) equilibrium is a fundamental concept for confined nuclear fusion and tokamak plasma equilibrium, in the presence of toroidal rotation. The set of fundamental equations of stationary MHD [6,11] provides a general description of plasma fluid under magnetic induction, namely the conservation of mass (1), the conservation of momentum (2), Gauss's law (3), Ampere's law (4), Ohm's law (5) and the thermodynamics laws (6,7,8),

$$\overrightarrow{\nabla} \cdot (\rho \overrightarrow{v}) = 0, \tag{1}$$

$$\rho \left(\overrightarrow{v} \cdot \overrightarrow{\nabla}\right) \overrightarrow{v} = \overrightarrow{J} \wedge \overrightarrow{B} - \overrightarrow{\nabla} P, \tag{2}$$

$$\overrightarrow{\nabla} \cdot \overrightarrow{B} = 0, \tag{3}$$

$$\mu_0 \overrightarrow{J} = \overrightarrow{\nabla} \wedge \overrightarrow{B}, \tag{4}$$

$$\overrightarrow{\nabla} \wedge (\overrightarrow{v} \wedge \overrightarrow{B}) = 0, \tag{5}$$

$$\overrightarrow{v} \cdot \overrightarrow{\nabla} S = 0, \tag{6}$$

$$P = \rho \overline{R} T, \tag{7}$$

$$P = A(S)\rho^{\gamma}, \tag{8}$$

where, P, m and T, are respectively, the mass, kinetic pressure and temperature of plasma. $\overrightarrow{B}$ is the magnetic induction, $\overrightarrow{J}$ is the current density, μ_0 is the vacuum magnetic permeability. The mass specific gas constant $\overline{R}$ represents the ratio of gas constant and the gas molecular weight. The caloric state equation in Eq. (8) is due to the fact that internal energy of the plasma considered as an ideal gas, is proportional only to the temperature, where A is function of the entropy S. The parameter γ represents the ratio of the two specific heats and has a value of $5/3$ for ideal monatomic gas.

Since tokamaks have an axisymmetric geometry, it is convenient to formulate the plasma equilibrium problem in a cylindrical coordinate system (r, φ, z), where (r, z) represents the poloidal plane section and φ the toroidal angle in the symmetric direction with $\overrightarrow{e}_{\varphi}$, the unit vector. Considering only a plane section at φ= constant, it easy to establish from Eq. (3), that the total magnetic field $\overrightarrow{B} = \overrightarrow{\nabla}\psi \wedge \overrightarrow{\nabla}\varphi + F\overrightarrow{\nabla}\varphi$, where $\psi = \iint_{\Omega} \overrightarrow{B}.\,\overrightarrow{n_{\rm P}}\; drdz$, is the poloidal flux function, $F = r\overrightarrow{B}.\overrightarrow{e}_{\varphi}$ is the diamagnetic function, Ω is the plasma domain and $\overrightarrow{n_{\rm P}}$ is the poloidal outgoing normal vector. The poloidal magnetic flux ψ can usefully describe the plasma equilibrium configuration and has nested magnetic surfaces. The compounds of the magnetic field are deduced as follows:

$$B_r = -\frac{1}{r}\frac{\partial \psi}{\partial z}, \quad B_z = \frac{1}{r}\frac{\partial \psi}{\partial r}, \quad B_{\varphi} = \frac{F}{r}. \tag{9}$$

The toroidal magnetic field, namely B_{φ}, is a key parameter in our algorithm, serving to properly adjust the equilibrium parameters.

In axisymmetric flow, and assuming for simplicity that the flow velocity is purely in the toroidal direction, *i.e.* $\overrightarrow{v} = v_{\varphi}\overrightarrow{e}_{\varphi}$, it is possible from Eq. (5), to establish that, $v_{\varphi} = r\omega(\psi)$, with ω is the toroidal rotation angular frequency of the flux surface.

Derivation of Eq. (2) with respect to Eqs. (6), (7) and previous relation, leads to,

$$\mu_0 \rho r^3 \omega^2 \overrightarrow{\nabla} r - \mu_0 r^2 \overrightarrow{\nabla} P = \left(\Delta^* \psi + F\frac{dF}{d\psi}\right)\overrightarrow{\nabla}\psi, \tag{10}$$

where, $\overrightarrow{\nabla}$ is the grad operator in poloidal plane section and the Laplacian-type symbol Δ^* has the form,

$$\Delta^* = r\frac{\partial}{\partial r}\left(\frac{1}{r}\frac{\partial}{\partial r}\right) + \frac{\partial^2}{\partial z^2}. \tag{11}$$

It is easy to establish from Eq. (10) that the pressure is function of ψ and r *i.e.*, $P \equiv P(\psi, r)$. Expansion of Eq. (10) with correlating its terms, leads to the following two separate relations,

$$-\Delta^* \psi = \mu_0 r^2 \frac{dP}{d\psi} + F\frac{dF}{d\psi} \tag{12}$$

$$\rho r \omega^2 - \left.\frac{\partial P}{\partial r}\right|_{\psi = cst} = 0, \tag{13}$$

where the derivative of P with respect to r is taken at constant ψ. We will present two solutions of Eq. (13) depending on the choice the functionals of ψ.

The equilibrium problem is quite challenging because the GGS equation involves several functionals of ψ, namely, $P(\psi), T(\psi), \omega(\psi), F(\psi)$ and $\rho(\psi)$. To further simplify the GGS equation, additional assumptions are needed, and the choice of these assumptions determines the nature of the solution.

The first solution follows the assumption proposed by [8], where the term $(\rho\omega^2)$ does not explicitly depend on the position r and is a functional of ψ. Assuming that the density is constant on magnetic surfaces, *i.e.*, $\rho = \rho(\psi)$ and $\omega = \omega(\psi)$, thus in this case the integration of the Eq. (13) leads to:

$$P(\psi, r) = \overline{P}(\psi) + \rho\omega^2 \frac{r^2}{2},$$

$$\Rightarrow P' = \overline{P}' + (\rho\omega^2)' \frac{r^2}{2}. \tag{14}$$

The prime denotes the derivative with respect to the poloidal flux function ψ. $\overline{P}(\psi)$ is the static pressure depending only on the poloidal flux ψ. This form clearly separates the centrifugal contribution of plasma rotation from the total pressure.

In this case, the Eq. (12) lead to following form:

$$-\Delta^* \psi = \mu_0 r^2 \frac{d\overline{P}}{d\psi} + \mu_0 \frac{r^4}{2}\frac{d(\rho\omega^2)}{d\psi} + F\frac{dF}{d\psi}. \tag{15}$$

Although the resulting pressure expression is simpler, the computation of the particular solution to the previous PDE depends on the chosen velocity profile. As reported in Ref. [8], a nonlinear profile based on $(\rho\omega^2)'$ was proposed.

This simplified expression of pressure introduces challenges, given the nonlinearity of the profile, when seeking an analytical solution - a fundamental requirement for the development of our algorithm. Nonetheless, it does not pose difficulties in the numerical resolution process, where such explicit forms can be readily implemented for the GSS equation.

The second solution follows the assumption where, the entropy is assumed to be constant at the magnetic surface, as cited in Refs. [6,18] also in Green and Karlson works [27], and the plasma temperature should depend on the flux function, *i.e.* $T = T(\psi)$. This last assumption implies that the thermal conductivity of the plasma is greater along the magnetic lines than between them. Using the Eq. (7), the integration of Eq. (13) with the integration constant chosen at $r = R_0$ for convenience, leads to,

$$P = \overline{P}(\psi)\exp\left(\frac{\omega^2}{2\overline{R}T}(r^2 - R_0^2)\right). \tag{16}$$

In the following development, we opted for the more general solution (16) of Eq. (13), which enables us to obtain the analytical expressions needed to effectively develop and validate our algorithm. Thus, our approach preserves the general form to facilitate analytical development while ensuring numerical tractability within the finite element framework.

General equilibrium equation with purely toroidal rotation, over a closed plasma domain is established by substituting eq. (16) into eq. (12),

$$-\Delta^*\psi = F\frac{dF}{d\psi} + \mu_0 r^2\left[\frac{d\overline{P}}{d\psi} + \overline{P}\frac{(r^2-R_0^2)}{2\overline{R}}\frac{d}{d\psi}\left(\frac{\omega^2}{T}\right)\right] \times \exp\left(\frac{\omega^2}{2\overline{R}T}(r^2-R_0^2)\right). \tag{17}$$

The toroidal Mach number, M, is defined as the ratio of the plasma toroidal velocity, v_φ, to the sound speed, C_s,

$$M = \frac{v_\varphi}{C_s}\ ,\quad C_s = \left(\frac{\partial P}{\partial \rho}\right)^{\frac{1}{2}}_{S=cst} \Rightarrow M^2 = \frac{r^2\omega^2}{\gamma \overline{R}T}$$
$$\omega(\psi, r) = \sqrt{\frac{\gamma P(\psi,r)}{\rho}}\frac{M}{r},\quad P(\psi,r) = \frac{\rho}{\gamma}\frac{v_\rho^2}{M^2}. \tag{18}$$

According to Maschke and Perrin works [6], for positive value of internal energy, $M^2 < 2/(\gamma-1)$, hence $M^2 < 3$.

The equilibrium problem is quite challenging because the GGS equation involves $F(\psi)$, $\overline{P}(\psi)$, $\omega(\psi)$ and $T(\psi)$. Solving the Eq. (17) requires prior knowledge of these profiles. To reduce the complexity, certain assumptions were made: the toroidal frequency ω and the temperature T were considered constant on each magnetic surface.

As a result, the GGS equation accounting for toroidal flow is expressed in this way.

$$-\Delta^*\psi = \mu_0 r J_\varphi,$$
$$J_\varphi = r\frac{d\overline{P}}{d\psi}\exp\left(\frac{\omega^2}{2\overline{R}T}(r^2-R_0^2)\right) + \frac{F}{\mu_0 r}\frac{dF}{d\psi}, \tag{19}$$

where J_φ denotes the toroidal current source. Since F does not include the Mach number, it can be consistently used as a constraint for any Mach number.

3. Plasma computational domain

The computational domain is established by designating a fixed boundary, chosen in our code as the outermost closed flux surface. This boundary is parametrized using Müller's formula [25,26] for Dshape plasmas, which is expressed as follows,

$$r = R_0 + a\cos\left(\theta + \arcsin(\delta)\sin(\theta)\right), \tag{20}$$
$$z = \kappa a \sin(\theta), \tag{21}$$

where R_0 and a represent the major and minor radius, respectively, $\epsilon = a/R_0$, the inverse aspect ratio, κ, the elongation,

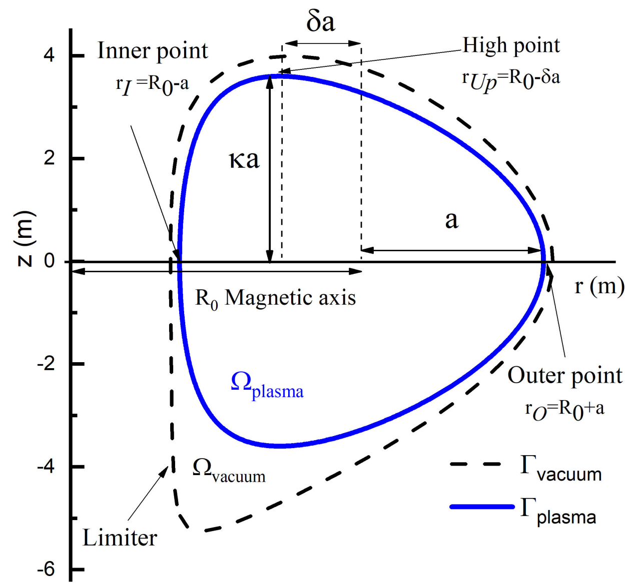

FIGURE 1. Computational plasma domain by Müller parametrization and locations of the higher, inner and outer points in a typical plasma boundary. These points are used to define the shaping parameters in Eqs. (20) and (21): the major and minor radius, elongation and triangularity.

δ, the triangularity and again the poloidal angle $\theta \in [0, 2\pi]$. The Fig. 1 shows the points that determine the height and the major and minor radius on a typical plasma border. It is generally possible to solve problem in an open domain, by setting an artificial computational boundary Γ_V located at a finite distance from the plasma border. A single or double null configuration can be achieved by following the strategy proposed in Ref. [28].

4. Exact solution of the GGS equation

Typically, the profiles of plasma pressure and diamagnetic functions are chosen to ensure that the source term vanishes at the plasma boundary, thereby modeling the effect of a perfectly conducting wall, as in the case of Solovev:

$$\mu_0\overline{P} = P_0\left(\psi - \psi_b\right),\ F^2 = 2F_0\left(\psi - \psi_b\right), \tag{22}$$

where ψ_b is the flux function at the plasma boundary, P_0 and F_0 are free parameters which can be tuned to constrain the specified equilibrium, this will be discussed further below.

The exact solution (ψ_{exact}) of the GGS given in Eq. (19) is the sum of vacuum (ψ_v) and particular (ψ_P) solutions. Zheng and *et al.* in Ref. [29] proposed a homogeneous solution satisfying the equation $-\Delta^*\psi_v = 0$, with general arbitrary polynomial degree, having up-down symmetry. By truncating the series, the solution is then written for $n = 4$ as follows,

$$\psi_{\text{exact}}(r,z)=\sum_{i=1}^{n} c_i\psi_i+P_0\left(\frac{R_0^2}{\gamma M_0^2}\right)^2\left[1+\frac{\gamma M_0^2}{2R_0^2}(r^2-R_0^2)\right.$$
$$\left.-\exp\left(\frac{\gamma M_0^2}{2R_0^2}(r^2-R_0^2)\right)\right]-\frac{F_0}{2}z^2. \tag{23}$$

where c_i are the constants computed from boundary conditions and the basic functions are $\psi_1 = 1$, $\psi_2 = r^2$, $\psi_3 = \left(r^4 - 4r^2z^2\right)$ and $\psi_4 = r^2\ln(r) - z^2$. Note that, the second term of Eq. (23) represents the particular solution and satisfies the GS equation with flow. We have introduced in Eq. (19), additional simplification, $\omega^2/\overline{R}T = \gamma(M_0^2/R_0^2) =$ cst, with M_0, the Mach number at the major radius $r = R_0$.

The equilibrium profiles are determined by imposing a Dirichlet condition on the plasma boundary, setting $\psi = \psi_b = 0$. To enforce this constraint, key extremal points on the boundary - the inner point (r_I), the outer equatorial point (r_O), and the uppermost point (r_{Up}) - are selected, as illustrated in Fig. 1. Owing to the up-down symmetry and the resulting redundancy, a Neumann condition is additionally imposed to ensure a net zero magnetic flux [19].

$$\begin{cases} \psi(R_0+a,0) & =\psi_b, \\ \psi(R_0-a,0) & =\psi_b, \\ \psi(R_0-\delta a,\kappa a) & =\psi_b, \\ \frac{1}{r}\frac{d\psi}{dr}\Big|_{\substack{r=r_{Up}=R_0-\delta a,\\ z=b=\kappa a}} & =0. \end{cases}$$

Using the boundary conditions, the Appendix A shows the mathematical derivations of the analytical expressions of the constants $\left(c_i,\ i=\overline{1,4}\right)$ for the exact solution of the GGS equation with flow. The calculation of c_i is a linear algebraic problem, involving four unknowns and it is trivial computationally. As we can see in Appendix A, all the constants c_i are found in terms of the geometrical parameters (R_0, a, κ, δ) describing the plasma cross section, the Mach number and the free parameters P_0 and F_0 of current density.

5. Numerical method

5.1. Problem specification

Numerical solution is carried out using the FEM applied to a matrix system derived from the variational principle. The numerical implementation employed FreeFEM++ [30], an open-source C++ environment for nonlinear partial differential equations (PDE) (`https://www.freefem.org/ff++/`).

$$\iint_\Omega \vec{\nabla}\psi\times\vec{\nabla}v\,dS+\iint_\Omega\frac{1}{r}\frac{\partial\psi}{\partial r}\,v\,dS$$
$$=\iint_\Omega\left[P_0r^2\exp\left(\frac{\gamma M_0^2}{2R_0^2}(r^2-R_0^2)\right)+F_0\right]v\,dS. \tag{24}$$

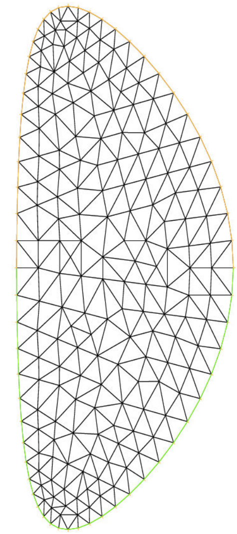

FIGURE 2. Subdivision of computational plasma domain "meshing".

The PDE given in Eq. (19) is cast in its weak form (integral) via the variational principle, with ψ and v the unknown poloidal function and test function, respectively and dS the surface element of plasma domain.

The boundaries are defined parametrically, and the mesh (with node connectivity) is generated automatically. FreeFEM++ provides an adaptive mesh generator. We subdivided the computational domain with P3 (cubic, third-order) elements (Fig. 2). For each element, the surface integrals of the basis functions in Eq. (24) are computed, yielding a linear matrix system for the poloidal flux, as $A\psi = B$. Free FEM++ provides both direct and iterative linear solvers and in this simulation, a direct solver was used; if the current source depended nonlinearly on ψ, an iterative approach would be more adequate.

5.2. Algorithm

The code computes both the exact and FEM solutions of Eq. (19). To fix the two free parameters P_0 and F_0 [Eq. (23)], we impose: (i) the computed on-axis toroidal field named B_ρ using the Eq. (9), equals the measured value ($B_0 = 2.25$T for JT-60SA chosen as the test), and (ii) the global error in Hilbert space between exact and numerical solutions of GGS equation solutions is minimized. For each Mach number, P_0 and F_0 are updated via two nested iterations: at each step, these parameters are adjusted so that the recalculated B_ρ, equals the measurement, B_0, and the relative error between successive iterates falls below a prescribed stopping error, named Tol (held fixed to 0.08%). This error, defined in Hilbert space [30], serves both as the stopping criterion and as the metric for alignment of the two solutions.

$$Error=\left(\frac{\iint_\Omega\left(\psi_{\text{exact}}-\psi_{\text{FEM}}\right)^2 d\Omega}{\iint_\Omega\psi_{\text{exact}}^2 d\Omega}\right)^{\frac{1}{2}}. \tag{25}$$

In summary, the inner (minor) loop of our algorithm manages the global error between the analytical and numerical solutions, while the outer (major) loop controls the value of the TMF. The input data consist of the toroidal magnetic flux at magnetic-axis and the toroidal Mach number. On an Intel Core i7 processor, the computation completes within 8 minutes.

Once the free parameters ensuring equilibrium have been determined, the solution is then consistently calculated, allowing the specification of many important physical quantities. These include, the total toroidal plasma current ($I_{\rm P}$), the ratio between the average particle pressure in the volume and the average poloidal magnetic field pressure along the plasma boundary ($\beta_{\rm P}$), the toroidal beta ($\beta_{\rm T}$), the normalized beta ($\beta_{\rm N}$), the safety factor at 95% of the plasma surface (q_{95}), and the plasma internal inductance (l_i):

$$I_{\rm P} = \iint_{\Omega} J_{\varphi} r dr dz, \tag{26}$$

$$\beta_{\rm P} = 2\mu_0 \frac{\langle P \rangle}{\overline{B_{\rm P}^2}}, \tag{27}$$

$$\beta_{\rm T} = 2\mu_0 \frac{\langle P \rangle}{B_0^2}, \tag{28}$$

$$\beta_{\rm N} = \beta_{\rm T} \frac{a B_0}{I_{\rm P}}, \tag{29}$$

$$q_{95} = \epsilon \frac{B_0}{\mu_0 I_{\rm P}} \oint_{\Gamma_{\rm P}} dl, \tag{30}$$

$$l_i = 4 \frac{\langle \frac{B_{\rm P}^2}{2\mu_0} \rangle}{\mu_0 I_{\rm P}^2 R_0}, \tag{31}$$

where B_0 is on-axis toroidal field and $B_{\rm P}$ is the poloidal magnetic field at the edge, the meaning of the symbols is

$$\langle \cdot \rangle = \frac{\iint_{\Omega} \cdot r dr dz}{\iint_{\Omega} r dr dz} \quad \text{and} \quad \overline{\cdot} = \frac{\oint_{\Gamma_{\rm P}} \cdot dl}{\oint_{\Gamma_{\rm P}} dl}.$$

$$\beta_P = 2\mu_0 \frac{\langle P \rangle}{[\frac{\mu_0 I_P}{\oint dl}]^2}, \quad \langle P \rangle = \frac{\iint_{\Omega} P(\psi, r) r dr dz}{V_P}$$

$$\Rightarrow \beta_P = \frac{2\mu_0}{[\frac{\mu_0 I_P}{\oint dl}]^2} \frac{\iint_{\Omega} P(\psi, r) r dr dz}{V_P}, \tag{32}$$

where V_p represents the total plasma volume (given in Table I). The relationship between the poloidal beta factor and the toroidal velocity is determined through the previous equation. As a complement to this work, we have provided in Appendix B, the mathematical development to explicitly derive the relationship between the poloidal beta and the toroidal velocity.

Note that the FEM evaluation of all surface and curvilinear integrals in the above expressions must be performed with care both within the plasma domain and along the closed constant-flux boundary.

The algorithm performed the following steps:

ALGORITHM.

Input data: $R_0,\ a,\ \delta,\ \kappa,\ M_0,\ B_0$ and $k_{\max}$: maximal number of iterations.
Output data: ψ_{exact}: analytical flux surface,
ψ_{FEM}: numerical flux surface,
$Error$, Tol, $I_{\rm P}$, $\beta_{\rm P}$, $\beta_{\rm T}$, $\beta_{\rm N}$, q_{95}, l_i and ω.

```
Set: P_0 = 0., ΔP_0 = 0.001, ΔF_0 = 0.001
▷ Initial values of free parameters.
for i = 1  to  k_max
F_0 ← 0.
Compute the constants (c_1, c_2, c_3, c_4)
for initial values of current free
parameters (Appendix A).
Compute the exact solution of GSTR Eq. (23).
Specify the source term J_φ and calculate
the numerical solution of GSTR Eq. (19).
Compute Error Eq. (25).
Tol ← Error.
for k = 1  to  k_max
F_0 ← F_0 + ΔF_0.
Update the calculation of (c_1, c_2, c_3, c_4)
(Appendix A).
Update the calculation of exact solution Eq. (23).
Update the source term J_φ and calculate again
numerical solution of GSTR Eq. (19).
Update Error in Eq. (25).
if (Error ≤ Tol) then:
Tol ← Error        ▷ Update the tolerance.
else
break        ▷ The tolerance is reached.
end if
end for
Compute ψ at r = R_0.
Compute B_ρ from the diamagnetic function F,
at r = R_0        ▷ Using the Eq. (9)
if (|B_ρ − B_0| > 10^−3) then:
P_0 ← P_0 + ΔP_0        ▷ Incrementation
of free parameter
else
break        ▷ Total toroidal magnetic
field achieved
end if
end for
Post-processing: compute the physical quantities
at the equilibrium Eqs. (26-31).
End program.
```

TABLE II. Computed equilibrium parameters of JT-60SA full plasma current inductive, for several values of Mach number at major radius.

	JT-60SA					Experimental values [20]
M_0	0.1	0.2	0.3	0.4	0.5	
$I_{\rm P}$(MA)	5.6285	5.5196	5.3623	5.1905	5.0134	5.5
q_{95}	2.7762	2.8348	2.9184	3.0134	3.1201	~ 3
l_i	0.7465	0.7445	0.7415	0.7375	0.7330	[0.8-1]
$\beta_{\rm T}(\%)$	7.5690	7.0120	6.2541	5.4325	4.6213	6.5
$\beta_{\rm P}$	0.8996	0.8669	0.8168	0.7550	0.6859	0.81
$\beta_{\rm N}$(m T/MA)	3.5703	3.3728	3.0965	2.7787	2.4473	3.1
B_ρ(T)	2.2498	2.2493	2.2490	2.2498	2.2493	2.25
Error$_{B_\rho}$(%)	0.0089	0.0311	0.0444	0.0089	0.0311	-

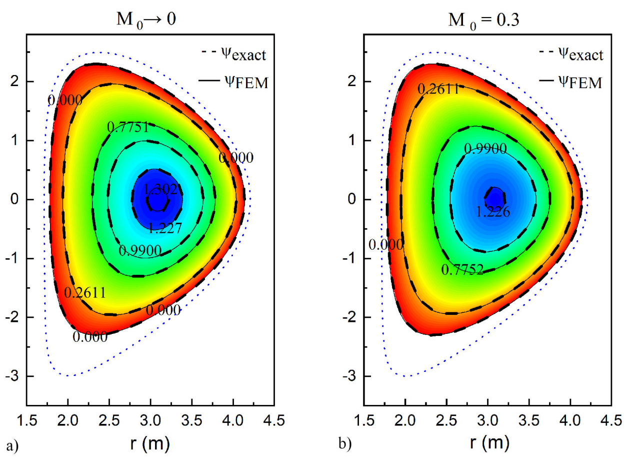

FIGURE 3. Poloidal flux surface of JT-60SA plasma. The dashed line represents the exact solution and the solid line corresponds to numerical one, a) for $M_0 \to 0$ and b) $M_0 = 0.3$.

6. Tests and benchmarking

To validate our results and to confirm the accuracy of the algorithm, we made a benchmark comparison between our analytical and numerical results, by using the spatial configuration of the JT-60SA full $I_{\rm P}$.

Figure 3 displays the flux contours for $M_0 \to 0$ (static case) and $M_0 = 0.3$, where, the simulation data have been taken from Table I. The comparison between the analytical and numerical solutions reveals a good agreement with a stopping error of Tol $= 10^{-3}$. The poloidal flux increases monotonically towards the magnetic axis, reaching a maximum value.

Table II displays the computational results of the equilibrium parameters of the JT-60SA full plasma current at several values of M_0, by using the programming code. Table II shows that the Mach number value corresponding to the operational parameters for JT-60SA, was found to be between [0.2-0.3]. This result in a good agreement with the relatively weak neutral beams used for the plasma heating as reported in Ref. [24].

The validation described above, shows that our algorithm has successfully minimized the global relative error while keeping the total toroidal field constant. We have confirmed that our algorithm offers a unique equilibrium solution with a good accuracy, consistent and in good agreement with the experimental data. Furthermore, we have also checked that, when the Mach number gets close to zero, our code can generate Solovev's equilibrium without the toroidal rotation.

7. Results and interpretations

In the following, we will examine the effect of toroidal flow on some physical profiles of the JT-60SA plasma at equilibrium. Authors in Refs. [5,31,32] have indicated that the actual Mach number in various reactor experiments should be

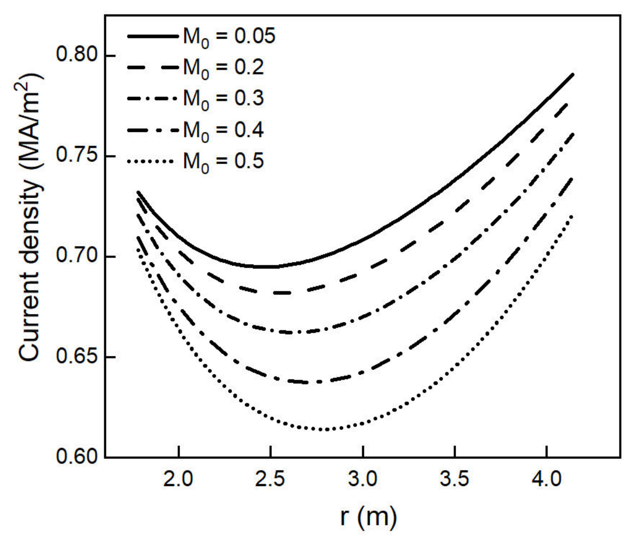

FIGURE 4. Radial profile of current density on the midplane, for several values of M_0.

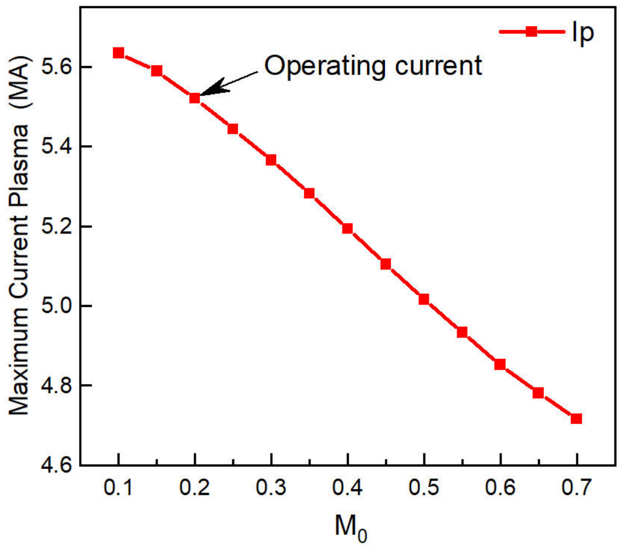

FIGURE 5. Evolution of the plasma current of JT-60SA as function of Mach number.

within the range of $[0.1 - 0.5]$ for plasma stability. So, in order to stay aligned with conventional values, we have selected M_0 in the range of $[0.1 - 0.7]$.

Radial evolution of the current density J_φ calculated on the median plane, exhibits a nonlinear distribution with a minimum, positioned at $r = R_0$ for a low Mach number as shown in Fig. 4. When M_0 increases, the value of the current density at the center decreases and its position can be slightly adjusted to achieve force balance. In addition, the minimum position of J_φ moves to the outer edge and the curve becomes more symmetric. According to Eq. (19), J_φ is proportional to the derivative of P and the square of F, the result being that the plasma center has a lower current density due to high pressure and high toroidal function, resulting in reverse shear equilibrium. The parameter F_0 plays an important role in reducing current density, especially in areas with a strong magnetic field.

The total plasma current I_P could be measured experimentally either computed numerically from the current density J_φ in the toroidal direction. As shown in Fig. 5, the most notable M_0 effect is the drop in current from 5.63 to 4.71 MA when M_0 goes from 0.1 to 0.7. This current evolution is shown by the results presented in Table II. Therefore, when there is some increase in toroidal rotation, control of the initial geometric profiles and the total toroidal field leads to a decrease in plasma current.

Maximum flux surface (ψ_max) and its shift position (Δ) are both displayed in Fig. 6a). The volume-averaged pressure ($\langle P\rangle$) with the shift position of P_max are reported in Fig. 6b). It is evident that, in addition to the reduction of the magnetic surface function, there is no change in the position of the maximum poloidal flux, as seen in Fig. 6a). Toroidal rotation creates a centrifugal force, as described by the first term in Eq. (2). This outward pushing force is counteracted by a reduction in plasma pressure, which brings the plasma column back to its initial position. Pustovitov's work [13] has proved that rotational velocity has no significant effect on the GS shift. By manipulating the parameter M_0, we can reduce the contribution of the pressure terms and achieve this result. The algorithm guarantees this operation. Similarly, the Fig. 6b) shows that as M_0 increases, the value of $\langle P\rangle$ decreases and reaches 111.71 kPa at $M_0 = 0.2$. We have compared this result by calculating $\langle P\rangle$ from the electron and ion energies, which we have found to be $\langle T_\mathrm{e}\rangle = \langle T_\mathrm{i}\rangle = 6.3$ keV (see Table I), with the data simulation $\rho = n{\times}2.5{\times}m$, $n = 0.56{\times}10^{20}\mathrm{m}^{-3}$, $m = 1.67{\times}10^{-27}$ kg and $\overline{R} = 3305.96$ J/(kg K). Equation (7) yields a value of 112.9 kPa with a relative error of 1%. Our code have provided a good result even when the operating parameters weren't exactly at $M_0 = 0.2$. The shift Δ increases nonlinearly with M_0 as predicted by Maschke and Perin's theoretical work [6].

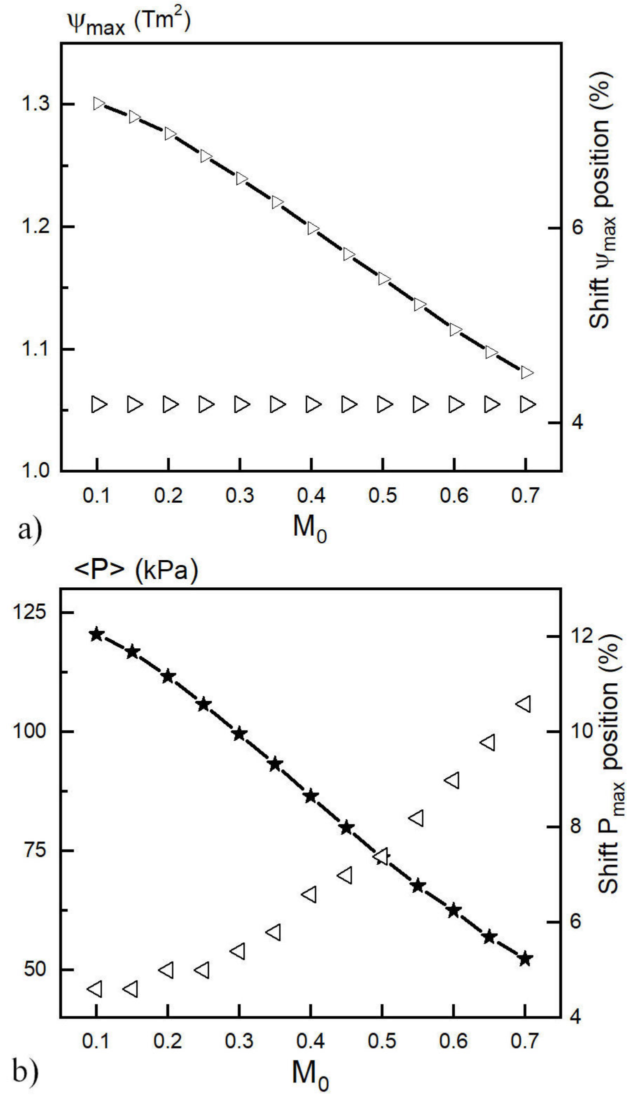

FIGURE 6. a) Effect of the toroidal rotation on maximum magnetic flux surface and its shift position and b) average pressure and shift position of maximum pressure.

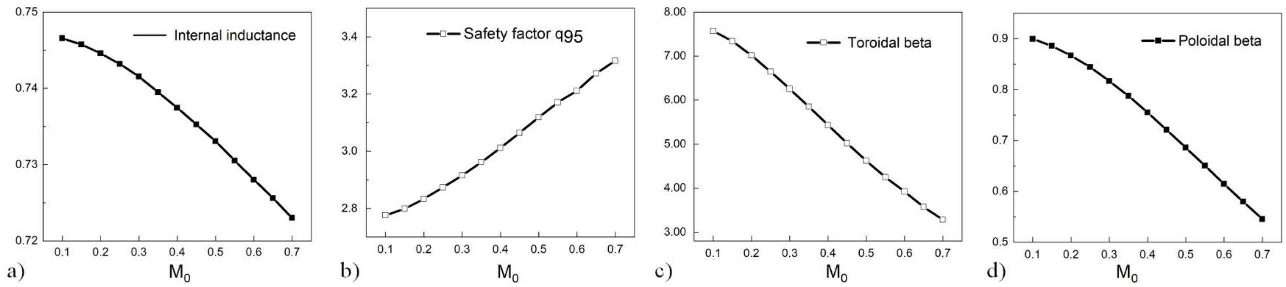

FIGURE 7. Effect of toroidal rotation on physical quantities, a) internal induction, b) safety factor q_{95}, c) toroidal beta and d) poloidal beta.

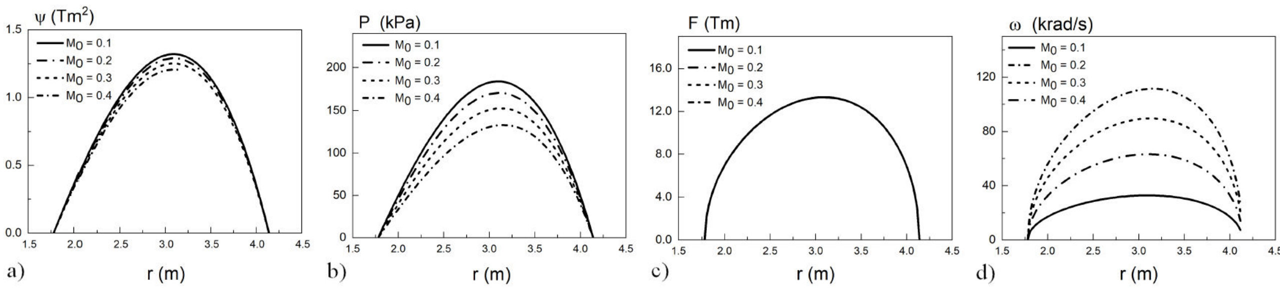

FIGURE 8. Several equilibrium profiles upon radial position of JT-60SA plasma, a) poloidal flux $\psi(r,0)$, b) plasma pressure $P(r,0)$, c) toroidal function $F(r,0)$ and d) toroidal frequency $\omega(r,0)$, all computed in the z-axis and for $M_0 = 0.1$, 0.2, 0.3 and 0.4.

The parameters as plasma internal induction, betas and safety factors are also affected by M_0, as shown in Fig. 7. The choice of current density terms resulted in paramagnetic plasma with $\beta_{\rm P}$ less than 1. Poloidal beta decreased slowly from 0.89 to 0.54, as seen in Fig. 7d), guaranteeing hence plasma stability, otherwise thermal pressure would cause the plasma to grow and move in the vacuum chamber until confinement was lost. The evolution of $\beta_{\rm P}$ is similar to that reported in Ref. [33]. Furthermore, Ilgisonis in Ref. [34], reported that toroidal rotation causes an increase of the equilibrium β limit, by 1.6 to 2.5 times compared to the static equilibrium. We have shown that this statement is incorrect and that our results lign with those of Pustovitov [13]. In fact, the equilibrium beta limit for a rotating plasma should be lower than that for a non-rotating plasma.

In high-beta plasma, toroidal beta dominates the total beta which is then equal to $\beta_{\rm T}$. Indeed, plasma $\beta_{\rm T}$ is often expressed in terms of $\beta_{\rm N}$, an operational parameter indicating how close the plasma is to reaching a non-equilibrium state. Similar variation of $\beta_{\rm T}$ is reported in Fig. 7c) where we can see that $\beta_{\rm T}$ decreases sharply from 7.83 to 4.78. In reality, the equilibrium must maintain fairly high beta values, and a necessary and sufficient condition for achieving high beta is to increase the pressure gradient (*i.e.* decrease ψ or increase P); paradoxically, this does not happen when toroidal rotation increases. No significant effect in the internal induction is observed in Fig. 7a), and our calculations resulted in l_i of 0.7 (70%) using Solov'ev equilibria. For this reason, l_i could potentially be used as a constraint parameter in the study in the presence of toroidal flow. Figure 7b) shows that M_0 increases the safety factor q_{95} parameter, which can be attributed to a reduction in the total plasma current.

Additional equilibrium profiles are plotted in Fig. 8, as function of radial position and at z-axis, namely, poloidal flux, plasma pressure, toroidal function, and toroidal rotation frequency at the center, all calculated for several values of M_0. All profiles show maximum value near the plasma center. The toroidal field function is not influenced by M_0 as indicated in Fig. 8c), since it is proportional to the total toroidal magnetic field B_0, which was maintained constant in the algorithm.

Figure 8d) shows how the toroidal frequency ω varies radially in the midplane. The toroidal velocity in tokamak experiments is usually maximum at the center of the plasma column. This is to be expected since the pressure is higher there. The toroidal velocity does not vanish at the outer edge of the plasma boundary, indicating a gradual transition beyond the confined region. From the Fig. 8d), we found $\omega = 62.69$ krad/s and $v_\rho = 62.69 \times 2.96 \simeq 180$ km/s, for $M_0 = 0.2$. We may compare by computing ω from the energy $T = 13.5$ keV (central electron temperature reported in Table I), which equates to $T = 156.65 \times 10^6$ K. By applying Eqs. (7) and (18), we obtain $\omega \simeq 62.77$ krad/s with 0.13% relative error.

Figure 9 is used for comparison with the results obtained using the FLOW code by Guazzotto [15]. Among the data reported in that work, the authors provided the midplane profile of v_ρ (which is proportional to ω) for an NSTX equilibrium. We plot the corresponding profile for JT-60SA at M_0 = 0.2 (operational mode). Although the two devices differ and the

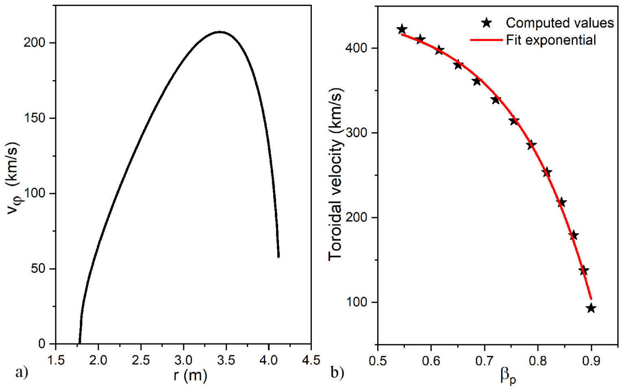

FIGURE 9. Midplane profile of toroidal velocity at $M_0 = 0.2$ (on left panel) and evolution of the toroidal velocity at center, upon poloidal beta (on right panel). Fitted curve of rotational velocity is: $v_\varphi = a + b \times \exp(c \times \beta_P))$, with $a = 448$, $b = -0.815$ and $c = 6.719$.

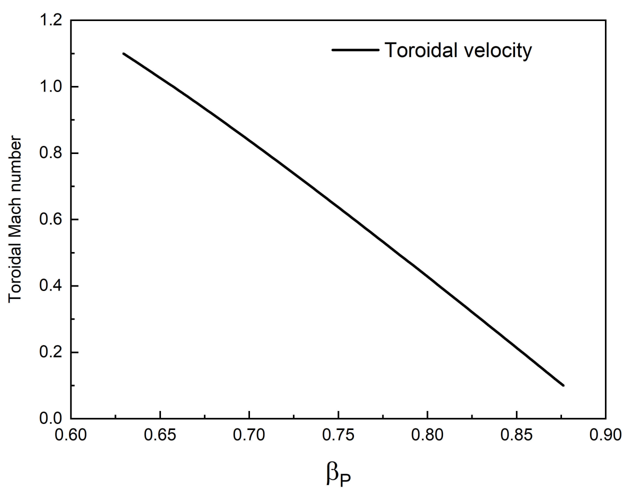

FIGURE 10. Relation between beta poloidal and toroidal velocity (through the Mach number) for $r = R_0$ for JT-60SA plasma.

absolute values are not directly comparable, both profiles exhibit similar behavior - notably, a rightward axial shift relative to the magnetic axis.

We have also plot in Fig. 9, v_ρ computed at R-axis, as function of poloidal beta. The evolution of the toroidal velocity is similar to that reported in Ref. [33]. Fitting the data points makes it possible to establish a direct relationship between the toroidal velocity and the poloidal beta. The curve is of form: $v_\varphi = a + b \times \exp(c \times \beta_{\mathrm{P}})$ with the coefficients $a = 448,\ b = -0.815$ and $c = 6.719$. This formula is useful from a theoretical and experimental point of view.

Figure 10 clearly illustrates the dependence of the toroidal velocity (through the Mach number) on the poloidal beta, and this result is consistent with that obtained by Nakamura [33]. The calculation was performed using the relation derived in Appendix B, evaluated at the point of maximum velocity, *i.e.*, in the vicinity of R_0. Although plasma pressure is described differently in our paper and in that of Nakamura [33] and Ivanov [8], the predictions obtained regarding the relationship between toroidal velocity and poloidal beta are similar.

8. Conclusion

In this work, we developed a numerical approach based on the finite element method to solve the Grad-Shafranov equation with toroidal flow. The implemented FEM algorithm, provides the magnetic configuration of 2D toroidally symmetric equilibria while maintaining the toroidal magnetic field (TMF) constant along the R-axis and equal to the measured value. The numerical results show a good agreement with the operating parameters, as validated against JT-60SA experimental data. The proposed algorithm yields a reconstruction error of approximately 0.1% for the poloidal flux function and less than 0.04% for the TMF. The effect of the toroidal Mach number was also studied using the same code, providing valuable insights into the control of plasma pressure, current, and rotation profiles. The most notable numerical prediction is that the plasma current (I_{P}) decreases as the toroidal flow increases. Future improvements to the proposed algorithm could include the implementation of free boundary conditions with coil effects, as well as a more precise treatment of magnetic field fluctuations.

Appendix A

Using new notations for the positions as follows: $r_O = R_0 + a,\ r_I = R_0 - a,\ r_{Up} = R_0 - \delta a$ and $b = \kappa a$,

$$\begin{cases} \psi\left(r_O, 0\right) = \psi_b, \\ \psi\left(r_I, 0\right) = \psi_b, \\ \psi\left(r_{Up}, b\right) = \psi_b, \\ \left.\frac{1}{r}\frac{d\psi}{dr}\right|_{\substack{r=r_{Up}\\ z=b}} = 0, \end{cases} \tag{A.1a}$$

$$\Rightarrow \begin{cases} \psi_h\left(r_O, 0\right) = \psi_b - \psi_P\left(r_O, 0\right), \\ \psi_h\left(r_I, 0\right) = \psi_b - \psi_P\left(r_I, 0\right), \\ \psi_h\left(r_{Up}, b\right) = \psi_b - \psi_P\left(r_{Up}, b\right), \\ \left.\frac{1}{r}\frac{d\psi_h}{dr}\right|_{\substack{r=r_{Up},\\ z=b}} = -\left.\frac{1}{r}\frac{d\psi_P}{dr}\right|_{\substack{r=r_{Up}\\ z=b}}, \end{cases} \tag{A.1b}$$

which it's can be written as linear system matrix $Ac = B$, with the matrix A and the vector unknown c,

$$A = \begin{pmatrix} 1 & r_O^2 & r_O^4 & r_O^2\ln(r_O) \\ 1 & r_I^2 & r_I^4 & r_I^2\ln(I_O) \\ 1 & r_{Up}^2 & r_{Up}^4 - 4r_{Up}^2 b^2 & r_{Up}^2\ln(r_{Up}) - b^2 \\ 0 & 2 & 4r_{Up}^2 - 8b^2 & 2\ln(r_{Up}) + 1 \end{pmatrix}, \tag{A.2a}$$

$c = \begin{pmatrix} c_1 & c_2 & c_3 & c_4 \end{pmatrix}^T$ and $B = \begin{pmatrix} B_1 & B_2 & B_3 & B_4 \end{pmatrix}^T$, with,

$$\begin{cases} B_1 = \psi_b - P_0\left(\frac{R_0^2}{\gamma M_0^2}\right)^2\left[1+\frac{\gamma M_0^2}{2R_0^2}(r_O^2-R_0^2)-\exp\left(\frac{\gamma M_0^2}{2R_0^2}(r_O^2-R_0^2)\right)\right], \\ B_2 = \psi_b - P_0\left(\frac{R_0^2}{\gamma M_0^2}\right)^2\left[1+\frac{\gamma M_0^2}{2R_0^2}(r_I^2-R_0^2)-\exp\left(\frac{\gamma M_0^2}{2R_0^2}(r_I^2-R_0^2)\right)\right], \\ B_3 = \psi_b - P_0\left(\frac{R_0^2}{\gamma M_0^2}\right)^2\left[1+\frac{\gamma M_0^2}{2R_0^2}(r_{Up}^2-R_0^2)-\exp\left(\frac{\gamma M_0^2}{2R_0^2}(r_{Up}^2-R_0^2)\right)\right]+\frac{F_0}{2}b^2, \\ B_4 = P_0\left(\frac{R_0^2}{\gamma M_0^2}\right)\left[1-\exp\left(\frac{\gamma M_0^2}{2R_0^2}(r_{Up}^2-R_0^2)\right)\right]. \end{cases} \tag{A.2b}$$

The four unknown constants are analytically determined using the Cramer method, with the determinant of matrix A expressed as follows:

$$\begin{aligned} \det[\mathrm{A}] = {} & r_I^2\left[4b^2r_O^2+(r_O^2-r_{Up})^2\right]\ln(r_I^2)-r_O^2\left[4b^2r_I^2+(r_I^2-r_{Up})^2\right]\ln(r_O^2)+(r_I^2-r_O^2)\Big[-8b^4-2b^2(r_I^2+r_O^2) \\ & +(r_I^2-r_{Up}^2)(r_O^2-r_{Up}^2)+(r_I^2r_{Up}^2-r_{Up}^2)\ln(r_{Up}^2)\Big]. \end{aligned} \tag{A.3}$$

The constants of the exact solution of the GGS are found as:

$$\begin{aligned} c_1 = {} & \Big[B_3r_I^2r_O^2(r_I^2-r_O^2)+8b^4(B_2r_O^2-B_1r_I^2)+b^2\big(2(B_2r_O^4-B_1r_I^4)+B_4r_I^2r_O^2(r_I^2-r_O^2)\big)+r_{Up}^2\big(B_2r_O^2(r_O^2-r_{Up}^2) \\ & +B_1r_I^2(r_{Up}^2-r_I^2)\big)+\frac{r_I^2}{2}\big(2B_3r_O^2(4b^2+r_O^2)-r_O^2r_{Up}^2(4B_3+B_4(4b^2+r_O^2))+r_{Up}^4(2B_1+B_4r_O^2)\big)\ln(r_I^2) \\ & +\frac{r_O^2}{2}\big(-2B_3r_I^2(4b^2+r_I^2)+r_I^2r_{Up}^2\times(4B_3+B_4(4b^2+r_I^2))-r_{Up}^4(2B_2+B_4r_I^2)\big)\ln(r_O^2) \\ & +\frac{1}{2}\big(2B_3r_I^2r_O^2(r_I^2-r_O^2)+B_4r_I^2r_O^2r_{Up}^2(r_O^2-r_I^2)+2(B_2r_O^2-B_1r_I^2)r_{Up}^4\big)\ln(r_{Up}^2)\Big]/\det[\mathrm{A}], \end{aligned} \tag{A.4}$$

$$\begin{aligned} c_2 = {} & \Big[8b^4\,(B_1-B_2)+(B_1-B_3)r_I^4+(B_3-B_2)r_I^4+b^2B_4(r_O^4-r_I^4)+(B_2-B_1)r_{Up}^4+\frac{r_I^2}{2}(8b^2(B_1-B_3) \\ & +B_4(r_O^4-r_{Up}^4)+4(B_3-B_1+b^2B_4)r_{Up}^2)\ln(r_I^2)+\frac{r_O^2}{2}(8b^2(B_3-B_2)+B_4(r_{Up}^4-r_I^4) \\ & +4(B_2-B_3-b^2B_4)r_{Up}^2)\ln(r_O^2)+\frac{1}{2}(2(B_1-B_3)r_I^4+2(B_3-B_2)r_O^4+B_4(r_I^4-r_O^4)r_{Up}^2 \\ & +2(B_1-B_2)r_{Up}^4)\ln(r_{Up}^2)\Big]/\det[\mathrm{A}], \end{aligned} \tag{A.5}$$

$$\begin{aligned} c_3 = {} & \Big[(B_1-B_2)(2b^2+r_{Up}^2)+r_I^2(B_3-B_1)+r_O^2(B_2-B_3)+b^2B_4(r_I^2-r_O^2)+\frac{r_I^2}{2}(2(B_1-B_3) \\ & +B_4(r_{Up}^2-r_O^2))\ln(r_I^2)+\frac{r_O^2}{2}(2(B_3-B_2)+B_4(r_I^2-r_{Up}^2))\ln(r_O^2)+\frac{1}{2}(2(B_2r_O^2-B_1r_I^2) \\ & +(r_I^2-r_O^2)(2B_3-B_4r_{Up}^2))\ln(r_{Up}^2)\Big]/\det[\mathrm{A}], \end{aligned} \tag{A.6}$$

$$\begin{aligned} c_4 = {} & \Big[2r_I^2(B_3-B_1)(r_I^2-2r_{Up}^2)+2r_O^2(B_2-B_3)(r_O^2-2r_{Up}^2)+(r_I^2-r_O^2)(B_4(r_I^2r_O^2-r_{Up}^2(r_I^2+r_O^2)+r_{Up}^4-4b^2r_{Up}^2) \\ & +8b^2B_3)+2(B_2-B_1)r_{Up}^4+8b^2(B_2r_O^2-B_1r_I^2)\Big]/\det[\mathrm{A}], \end{aligned} \tag{A.7}$$

Appendix B

The beta poloidal is defined as:

$$\beta_P = 2\mu_0 \frac{\langle P \rangle}{\left[\frac{\mu_0 I_P}{\oint dl}\right]^2}. \tag{B.1}$$

The plasma perimeter is approximated as follows:

$$L = \oint dl = 2\pi a \sqrt{\frac{1+\kappa^2}{2}}. \tag{B.2}$$

We have seen from the results obtained previously that the plasma velocity is maximal near $r = R_0$; therefore, we will derivate the formulas in the vicinity of R_0. Theses following expansions are carried out at $r \approx R_0$:

$$(r^2 - R_0^2) = (r - R_0)(r + R_0) = 2R_0(r - R_0) \Rightarrow \exp\left[\frac{\gamma M_0^2}{2R_0^2}(r^2 - R_0^2)\right] = \exp\left[\frac{\gamma M_0^2}{R_0}(r - R_0)\right]. \tag{B.3}$$

To simplify the expressions, let us set: $\alpha = \gamma M_0^2/R_0$.

B.1 The average pressure calculation

$$\langle P \rangle V_P = \iint_\Omega P r dr dz = \frac{1}{\mu_0} \iint_\Omega P_0 \psi_a \exp\left[\frac{\gamma M_0^2}{R_0}(r - R_0)\right] r dr dz. \tag{B.4}$$

The pressure is given through in Eq.(16) and Eq. (22). ψ_a is the magnetic flux at R-axis. The limits of integration are taken: $r = R_0 - a, R_0 + a$ et $z = -b, b$:

$$I_1 = \iint \exp\left[\frac{\gamma M_0^2}{R_0} r\right] r dr dz = 2b\left[\frac{r}{\alpha} - \frac{1}{\alpha^2}\right] \exp(\alpha r)\Big|_{R_0-a}^{R_0+a} \langle P \rangle V_P = \frac{2b}{\mu_0} P_0 \psi_a$$
$$\times \left[\frac{2}{\alpha}\Big(R_0 \sinh(\alpha a) + a\cosh(\alpha a)\Big) - \frac{2}{\alpha^2}\sinh(\alpha a)\right]. \tag{B.5}$$

B.2 The plasma current calculation

$$I_P = \frac{1}{\mu_0} \iint \left[r P_0 \exp\left[\frac{\gamma M_0^2}{R_0}(r - R_0)\right] + \frac{F_0}{r}\right] dr dz, \tag{B.6}$$

$$I_2 = \iint \exp\left[\frac{\gamma M_0^2}{R_0} r\right] r dr dz = 2b\left[\frac{r}{\alpha} - \frac{1}{\alpha^2}\right] \exp(\alpha r)\Big|_{R_0-a}^{R_0+a}, \tag{B.7}$$

$$I_3 = F_0 \iint \frac{dr dz}{r} = F_0 2b \ln\left(\frac{R_0 + a}{R_0 - a}\right). \tag{B.8}$$

The plasma current after developement lead to:

$$\mu_0 I_P = 2bP_0\left[\frac{a}{\alpha} 2\cosh(\alpha a) + \left(\frac{R_0}{\alpha} - \frac{1}{\alpha^2}\right) 2\sinh(\alpha a)\right] + F_0 2b \ln\left(\frac{R_0 + a}{R_0 - a}\right). \tag{B.9}$$

The final relation of poloidal beta expressed as follow:

$$\beta_P = \frac{2\mu_0}{V_P} \frac{\frac{2b}{\mu_0} P_0 \psi_a \left[\frac{2}{\alpha}\Big(R_0 \sinh(\alpha a) + a\cosh(\alpha a)\Big) - \frac{2}{\alpha^2}\sinh(\alpha a)\right]}{\left[2bP_0\left[\frac{a}{\alpha} 2\cosh(\alpha a) + \left(\frac{R_0}{\alpha} - \frac{1}{\alpha^2}\right) 2\sinh(\alpha a)\right] + F_0 2b \ln\left(\frac{R_0+a}{R_0-a}\right)\right]^2} \times (L)^2, \tag{B.10}$$

with

$$\alpha = \frac{\gamma v_\rho(R_0)^2}{R_0 C_s^2}. \tag{B.11}$$

This relation gives beta as a function of the toroidal velocity and clearly shows that if the velocity increases, then beta poloidal decreases. The calculation is performed using Python programming.

Author contributions

A. Djellouli and A.R. Senoudi wrote the main text of the manuscript, A. Djellouli performed the analytical solution of the GGS equation, A.R. Senoudi made the algorithm and performed the numerical solution with the finite element method. All authors prepared Figs. 1-10, and approved the submitted version.

Statements and declarations

Competing interests

The authors have no conflicts to disclose.

Funding

No funding was received for conducting this study.

Data availability

Authors do not have any research data outside the submitted manuscript file.

1. G. Ludwig, Direct variational solutions to the Grad-Schluter-Shafranov equation, *Plasma physics and controlled fusion* **37** (1995) 633.
2. V. Shafranov, On magnetohydrodynamical equilibrium configurations, *Soviet Physics JETP* **6** (1958) 1013.
3. R. Isler *et al*., Rotation scalings and momentum confinement in neutral-beam-injected ISX-b plasmas, *Nuclear fusion* **26** (1986) 391.
4. M. Bell, Measurements of plasma rotation in tokamak LT-3, *Nuclear Fusion* **19** (1979) 33.
5. R. Isler *et al*., Impurity transport and plasma rotation in the ISX-B tokamak, *Nuclear Fusion* **23** (1983) 1017.
6. E. Maschke and H. Perrin, Exact solutions of the stationary MHD equations for a rotating toroidal plasma, *Plasma Physics* **22** (1980) 579.
7. H.-P. Zehrfeld and B. Green, Stationary toroidal equilibria at finite beta, *Nuclear Fusion* **12** (1972) 569.
8. A. Ivanov *et al.*, Tokamak plasma equilibrium problems with anisotropic pressure and rotation and their numerical solution, Plasma Physics Reports **41** (2015) 203.
9. R. Iacono *et al*., Axisymmetric toroidal equilibrium with flow and anisotropic pressure (1989).
10. A. Ito and N. Nakajima, Equilibria of toroidal plasmas with toroidal and poloidal flow in high-beta reduced magnetohydrodynamic models, *Nuclear Fusion* **51** (2011) 123006.
11. J. P. Freidberg, ideal MHD (Cambridge University Press, 2014).
12. J. P. Sudano and L. S. Goes, Equilibrium of a toroidal plasma, *Theoretical and computational plasma physics* (1978) 483.
13. V. Pustovitov, Equilibrium of rotating and nonrotating plasmas in tokamaks, *Plasma Physics Reports* **29** (2003) 105.
14. H. Lütjens, A. Bondeson, and O. Sauter, The CHEASE code for toroidal MHD equilibria, *Computer physics communications* **97** (1996) 219.
15. L. Guazzotto *et al.*, Numerical study of tokamak equilibria with arbitrary flow, *Physics of Plasmas* **11** (2004) 604
16. J. Lee and A. Cerfon, ECOM: a fast and accurate solver for toroidal axisymmetric MHD equilibria, *Computer Physics Communications* **190** (2015) 72
17. X. Song, et al., Control-Oriented Free-Boundary Equilibrium Solver for Tokamaks, *Plasma* **7** (2024) 842.
18. H. Li and P. Zhu, Solving the Grad-Shafranov equation using spectral elements for tokamak equilibrium with toroidal rotation, *Computer Physics Communications* **260** (2021) 107264
19. A. J. Cerfon and J. P. Freidberg, "One size fits all" analytic solutions to the Grad-Shafranov equation, *Physics of Plasmas* **17** (2010)
20. Y. Kamada *et al.*, Plasma regimes and research goals of JT-60SA towards ITER and DEMO, Nuclear Fusion **51** (2011) 073011.
21. V. Mukhovatov *et al.*, Overview of physics basis for ITER, Plasma physics and controlled fusion **45** (2003) A235
22. M. Matsukawa *et al.*, Optimization of plasma initiation scenarios in JT-60SA, *J. Plasma Fusion Res. SERIES* **9** (2010) 264.
23. A. Aydemir, B. Park, and K. Han, Exact Solov'ev equilibrium with an arbitrary boundary, *Physics of Plasmas* **26** (2019).
24. R. Schmitt, et al., Free-boundary magnetohydrodynamic equilibria with flow, *Physics of Plasmas* **18** (2011).
25. R. Miller, et al., Noncircular, finite aspect ratio, local equilibrium model, *Physics of Plasmas* **5** (1998) 973.
26. T. Luce, An analytic functional form for characterization and generation of axisymmetric plasma boundaries, *Plasma physics and controlled fusion* **55** (2013) 095009.
27. J. M. Greene and E. T. Karlson, Variational Principale for stationary Magnetohydrodynamic Equilibria., Tech. rep., Princeton Univ., *NJ Plasma Physics Lab*. (1966).
28. D. Ciro and I. L. Caldas, A semi-analytical solver for the Grad-Shafranov equation, *Physics of Plasmas* **21** (2014).
29. S. Zheng, A. Wootton, and E. R. Solano, Analytical tokamak equilibrium for shaped plasmas, *Physics of plasmas* **3** (1996) 1176.
30. F. Hecht, New development in FreeFem++, *J. Numer. Math.* **20** (2012) 251.

31. Y. Hu, Y. Hu, and N. Xiang, Fixed boundary toroidal plasma equilibria with toroidal flows, *Physics of Plasmas* **23** (2016).
32. N. Hawkes and N. Peacock, Toroidal rotation in the DITE tokamak, *Nuclear fusion* **25** (1985) 971.
33. K. Nakamura, et al., Plasma equilibrium based on EC- driven current profile with toroidal rotation on QUEST, *Fusion Engineering and Design* **146** (2019) 2628.
34. V. Ilgisonis and Y. I. Pozdnyakov, Transport barrier as a bifurcation of the equilibrium of a tokamak plasma, *Plasma Physics Reports* **28** (2002) 83.